Environmental Science & Technology

Article

Cite This: Environ. Sci. Technol. 2019, 53, 4450−4459

pubs.acs.org/est

The Impact of pH and Irradiation Wavelength on the Production of Reactive Oxidants during Chlorine Photolysis

Devon Manley Bulman,[†] Stephen P. Mezyk,[‡] and Christina K. Remucal*[,†,§]

[†]Environmental Chemistry and Technology Program University of Wisconsin−Madison, Madison, Wisconsin 53706, United States
[‡]Department of Chemistry and Biochemistry California State University at Long Beach Long Beach, California 90840, United States
[§]Department of Civil and Environmental Engineering University of Wisconsin−Madison, Madison, Wisconsin 53706, United States

Supporting Information

ABSTRACT: Chlorine photolysis is an advanced oxidation process which relies on photolytic cleavage of free available chlorine (i.e., hypochlorous acid and hypochlorite) to generate hydroxyl radical, along with ozone and a suite of halogen radicals. Little is known about the impact of wavelength on reactive oxidant generation even though chlorine absorbs light within the solar spectrum. This study investigates the formation of reactive oxidants during chlorine photolysis as a function of pH (6−10) and irradiation wavelength (254, 311, and 365 nm) using a combination of reactive oxidant quantification with validated probe compounds and kinetic modeling. Observed chlorine loss rate constants increase with pH during irradiation at high wavelengths due to the higher molar absorptivity of hypochlorite (pK_a = 7.5), while there is no change at 254 nm. Hydroxyl radical and chlorine radical steady-state concentrations are greatest under acidic conditions for all tested wavelengths and are highest using 254 and 311 nm irradiation. Ozone generation is observed under all conditions, with maximum cumulative concentrations at pH 8 for 311 and 365 nm. A comprehensive kinetic model generally predicts the trends in chlorine loss and oxidant concentrations, but a comparison of previously published kinetic models reveals the challenges of modeling this complex system.

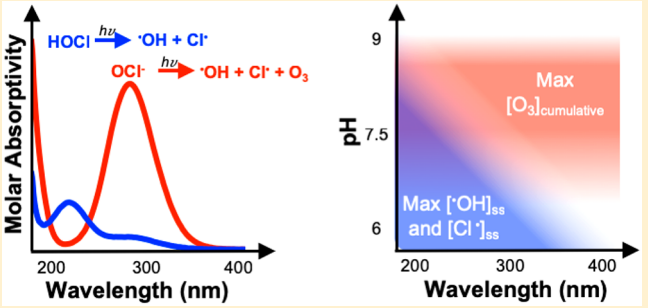

INTRODUCTION

The presence of organic contaminants, such as pesticides and pharmaceuticals, in drinking water sources poses a challenge to water utilities. These chemicals are released into the environment through municipal wastewater, agricultural runoff, and landfill leachate[1−8] and are often poorly removed by conventional water treatment processes.[9] In contrast, advanced oxidation processes (AOPs) can degrade a wide range of organic contaminants by producing hydroxyl radical (•OH), a highly reactive, nonselective oxidant that reacts with nearly all organic compounds at diffusion-controlled rate constants.[10−19] Traditional AOPs, such as hydrogen peroxide photolysis, require costly retrofits to existing plants and can be expensive to maintain due to the necessary quenching of hydrogen peroxide, among other factors.[18,20−25]

Chlorine photolysis is emerging as an attractive alternative to traditional AOPs. This system relies on the irradiation of free available chlorine (FAC), a combination of hypochlorous acid (HOCl) and hypochlorite (OCl^-), to generate reactive oxidants. While hydrogen peroxide and persulfate-based AOPs can only use light in the UV-C range due to limits in molar absorptivity,[26,27] solar treatment applications of chlorine photolysis are possible because HOCl and OCl^- absorb light at higher wavelengths.[14,28−30] Furthermore, chlorine photolysis utilizes a common disinfectant that is easily transported and the AOP is more cost-effective under many conditions compared to hydrogen peroxide and persulfate-based AOPs.[18,31]

The chemistry of chlorine photolysis is complex due to the wavelength dependent photolysis of chlorine and its subsequent oxidant formation mechanisms. The acid dissociation constant (pK_a) of hypochlorous acid is 7.5, making the photochemistry of both species important under environmentally relevant pH values.[32] Hypochlorous acid photolyzes to form •OH and chlorine radical (Cl•; Reaction 1 in Scheme 1).[33] Hypochlorite photolysis is more complex because it forms $O^{-\bullet}$, the conjugate base of •OH, as well as two excited states of oxygen, $O(^1D)$ and $O(^3P)$ (Reactions 2−4).[34] Additional reactive chlorine species (RCS) form during chlorine photolysis. For example, $Cl_2^{-\bullet}$ forms by reaction of Cl• with Cl^-, while ClO• forms by reaction of Cl• or •OH with chlorine. Cl• is more selective than •OH but reacts at near-diffusion controlled rates with electron-rich compounds.[35,36] $Cl_2^{-\bullet}$ and ClO• are generally less reactive compared to •OH and Cl•, but they react selectively with some organic

Received: December 21, 2018
Revised: March 18, 2019
Accepted: March 19, 2019
Published: March 19, 2019

DOI: 10.1021/acs.est.8b07225
Environ. Sci. Technol. 2019, 53, 4450−4459

Scheme 1. Literature Quantum Yields of Photolysis for Both HOCl and OCl^- at 254, 311, and 365 nm.[20,32−34,43]

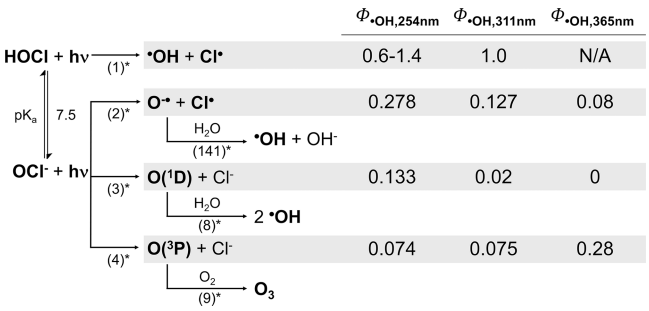

*Reaction numbers correspond to reactions in Table S2.

compounds (e.g., phenolates and methoxybenzenes).[37−41] $Cl^•$ and $Cl_2^{-•}$ may be considered problematic because these species could potentially form chlorinated disinfection byproducts via chlorine addition or substitution.[37,40−42]

While the presence of multiple potential oxidants makes chlorine photolysis effective at oxidizing a wide range of organic contaminants, it also makes the system challenging to study. Experimental studies rely on the use of probe compounds to quantify oxidant species. Nitrobenzene is frequently used as a selective $^•OH$ probe due to its photostability and low reactivity with other oxidants (i.e., HOCl and RCS).[22−24,33,40,44,45] Measurements of $Cl^•$ and $Cl_2^{-•}$ are infrequent but typically use benzoate in combination with nitrobenzene. Benzoate has literature rate constants with all three species, although there is debate about which reaction mechanisms (i.e., with $^•OH$, $Cl^•$, and/or $Cl_2^{-•}$) are dominant.[22,33,46]

Organic compound degradation during chlorine photolysis provides additional insight into the formation of reactive oxidants under 254 nm irradiation, which is the most studied wavelength. The fraction of contaminant lost to reaction with $^•OH$ is typically estimated by combining measured $^•OH$ steady-state concentrations with literature bimolecular rate constants after correcting for loss due to dark chlorination or direct UV photolysis,[23,37] and any remaining degradation is attributed to RCS. The relative impacts of multiple quenchers are used to assess the contribution of RCS to contaminant degradation, although this approach does not always generate meaningful results.[24] For example, the impact of *t*-butanol (i.e., a quencher of $^•OH$, $Cl^•$, and $ClO^•$) may be compared to the impact of bicarbonate (i.e., a quencher of $^•OH$, $Cl^•$, and $Cl_2^{-•}$).[14,23] As a result, $ClO^•$ is increasingly evoked as an important oxidant for organic compound degradation (e.g., naproxen, caffeine, trimethoprim, and microcystin-LR).[14,23,37,47] However, many of these compounds react with ozone,[48,49] which is overlooked in studies conducted at 254 nm and whose precursor (i.e., $O(^3P)$) is quenched by *t*-butanol.[28]

Understanding the formation of reactive oxidants is critical to the application of chlorine photolysis for water treatment. Importantly, results generated at 254 nm provide a limited view of chlorine photolysis and cannot be extrapolated to potential solar applications because quantum yields and reaction mechanisms change with irradiation wavelength (Scheme 1). Thus, we aim to determine how reactive oxidant generation varies with treatment conditions by quantifying the steady-state concentrations of $^•OH$ and $Cl^•$ and the cumulative concentration of O_3 as a function of pH and wavelength using a series of validated probes. We also develop a comprehensive kinetic model that we compare to five previously published models[22,29,33,40,46] to highlight the limitations of relying on kinetic models in the absence of experimental measurements.

MATERIALS AND METHODS

Materials. Sodium hypochlorite stock solutions were standardized using a Shimadzu UV−vis spectrometer.[32] All other compounds were used as received (Supporting Information Section S1).

Irradiation Experiments. Photolysis experiments were conducted in a Rayonet merry-go-round photoreactor with either four 254 nm bulbs, sixteen 311 nm bulbs, or sixteen 365 nm bulbs (Figure S1). These bulbs were selected because they represent different regions in the ultraviolet light spectrum and are not monochromatic light sources. Bulbs are identified by the λ_{max}. All experiments were conducted in triplicate alongside a chemical actinometer (*p*-nitroanisole/pyridine at 365 nm,[50−52] 2-nitrobenzaldehyde at 311 nm,[53] and sulfamethoxazole and diclofenac at 254 nm).[54] Bulb specifications and actinometer conditions are provided in Section S2. Error bars in all figures represent the standard deviation of triplicate analyses.

Irradiation experiments were conducted using 10 mM phosphate (pH 6−7) or borate (pH 8−10) buffer. The experimental duration varied with wavelength due to variance in bulb intensity (i.e., 2 min at 254 nm, 100 s at 311 nm, and 10 min at 365 nm). The pseudo-first-order rate constants of chlorine degradation were measured by photolyzing buffered solutions of chlorine (initial concentration = 4 mg-Cl_2/L) at pH 6−10 and 254, 311, and 365 nm.

Nitrobenzene, benzoate (pK_a = 4.19),[55] and cinnamic acid were selected as probe compounds for hydroxyl radical, RCS, and ozone, respectively, due to their specific reactivity and photostability at the irradiation wavelengths (Figure S2). Oxidant measurements were conducted at each pH and wavelength with 10 mM phosphate or borate buffer, 4 mg-Cl_2/L, and 10 μM probe.

Probe Validation. A series of experiments were conducted to assess the reactivity of nitrobenzene and benzoate with O_3, $^•OH$, $Cl^•$, $Cl_2^{-•}$, and $ClO^•$ under experimental conditions. First, solutions were purged with nitrogen to limit ozone formation[30,34] to confirm that reaction between the probes and O_3 is minimal. Second, chlorine photolysis experiments were conducted at low pH (i.e., pH 0.25), which is considered to be a clean source of $Cl^•/Cl_2^{-•}$,[32,44] to validate the selectivity of nitrobenzene for $^•OH$.[56] Third, the reactivity of benzoate with reactive halogen species was verified using competition kinetics with nitrobenzene. Finally, experiments were conducted with elevated chloride (0−500 mM) and chlorine (0.4−100 mg-Cl_2/L) to shift the RCS toward $Cl_2^{-•}$ and $ClO^•$, respectively, in order to identify which RCS react with benzoate. Details are provided in Section S3.

Analytical Methods. Chlorine concentrations were measured immediately using the *N*,*N*-diethyl-*p*-phenylenediamine colorimetric method.[57] Chloride and sulfate concentrations were measured using anion chromatography after quenching chlorine samples using 0.5 M sodium thiosulfate to determine the initial chloride concentration, where the initial concentration of chloride is the difference between sulfate and chloride after quenching.[58] The initial chloride concentration in 4 mg-Cl_2/L was 1.25×10^{-4} M. The loss of nitrobenzene

DOI: 10.1021/acs.est.8b07225
Environ. Sci. Technol. 2019, 53, 4450−4459

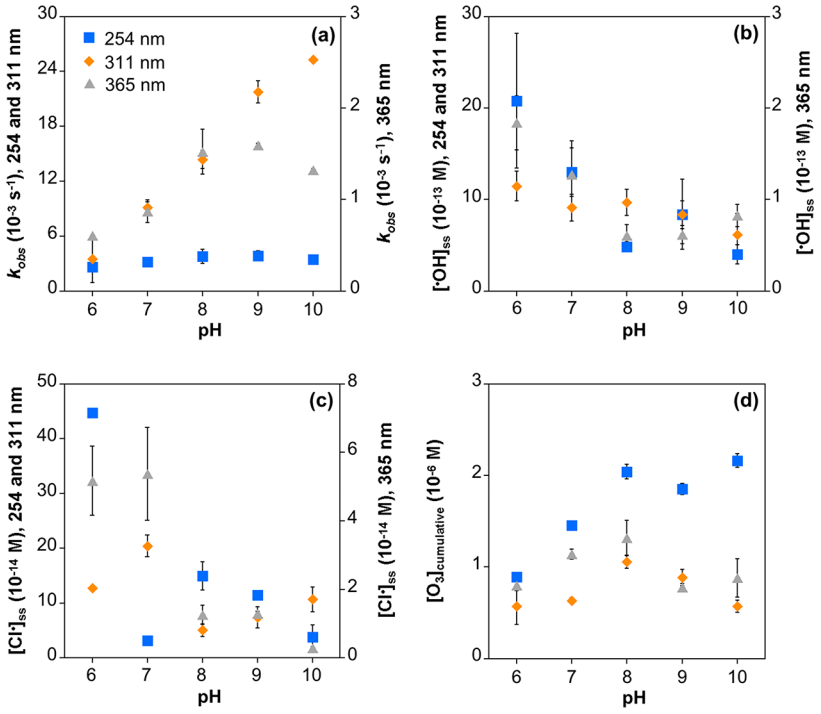

Figure 1. (a) Observed free chlorine loss rate constant, (b) hydroxyl radical steady-state concentration, (c) chlorine radical steady-state concentration, and (d) cumulative ozone formation as a function of pH during irradiation at 254, 311, and 365 nm (secondary axis).

and benzoate and formation of benzaldehyde were quantified by high-performance liquid chromatography (Section S4).

Kinetic Modeling. A kinetic model containing 196 elementary reactions was built using Kintecus 4.55.[59] The model was based on previous literature models[22,29,33,40,46] and was amended with additional rate constants from the literature (Table S2), including the formation and reaction of ozone. The model was compared with the results of previously published models that were rebuilt in Kintecus and run with the same input rates (Section S5).[22,29,33,40,46,59]

Rate Constant Measurements. The second-order rate constants of $^{\bullet}OH$ with HOCl and OCl^- were measured using electron pulse radiolysis and transient absorption spectroscopy (Section S6).

RESULTS AND DISCUSSION

Direct and Indirect Photolysis of Chlorine. Both the direct photolysis of chlorine and the subsequent formation of reactive oxidants are dependent on pH and wavelength. Therefore, identifying how chlorine loss rate constants respond to these parameters will improve our understanding of oxidant production. To determine the effect of pH and wavelength on chlorine degradation, the observed loss rate constant was quantified at pH 6−10 with 254, 311, and 365 nm irradiation. Chlorine degradation followed pseudo-first order kinetics, with observed rate constants ranging from 3.79×10^{-4} s^{-1} (365 nm, pH 6) to 2.53×10^{-2} s^{-1} (311 nm, pH 10).

Chlorine degradation was independent of pH at 254 nm (Figure 1a). This observation agrees with past work in which the observed chlorine loss rate constant does not change with pH under UV-C irradiation.[29,33,60,61] This effect may partially be explained by the relative molar absorptivities of the two chlorine species,[60,62] which are nearly equal at 254 nm (Figure S1). For example, the ratio of molar absorptivities is on the same order of magnitude as the ratio of $k_{obs,FAC}$ (A_{254,OCl^-}:$A_{254,HOCl}$ = 0.96; k_{obs,OCl^-}:$k_{obs,HOCl}$ = 1.32; Table S3). However, it is important to note that $k_{obs,FAC}$ includes both direct and indirect photolysis reactions (i.e., additional chlorine loss via reaction with $^{\bullet}OH$ or RCS). Since the quantum yields of $^{\bullet}OH$ formation from HOCl and OCl^- at 254 nm are similar (Scheme 1), k_{obs,OCl^-}:$k_{obs,HOCl}$ is greater than predicted based on molar absorptivities because $^{\bullet}OH$ reacts more quickly with OCl^- than with HOCl ($(6.37 \pm 0.06) \times 10^9$ and $(1.21 \pm 0.17) \times 10^9$ M^{-1} s^{-1}, respectively; Section S6). Relying on measured $k_{obs,FAC}$ to calculate quantum yields for Reactions 1−4 results in values >1 due to indirect photolysis reactions,[32,46,62−64] which are sometimes erroneously used in kinetic models in place of quantum yields of radical formation.[29,46]

The chlorine loss rate constant increased with pH at higher irradiation wavelengths (Figure 1a), which agrees with the trend observed under simulated sunlight and using UV-C and near UV-C irradiation.[29,60,61] OCl^- absorbs more light compared to HOCl at 311 and 365 nm (Table S3; Figure S1), yet the $^{\bullet}OH$ quantum yields from OCl^- are much lower than HOCl at these wavelengths (Scheme 1). Therefore, the difference in molar absorptivity (i.e., direct photolysis) is the dominant driver of the observed pH dependence of chlorine loss. Deviations from this trend are attributable to indirect photolysis of HOCl due to elevated steady-state concentrations of $^{\bullet}OH$ at lower pH values.

Validation of Probe Compounds. Nitrobenzene and benzoate are ideal reactive oxidant probes in chlorine photolysis systems because they are unreactive with chlorine[44] and do not undergo direct photolysis between 254 and 365 nm (Figure S2).[32,33,44] Furthermore, the reaction of both compounds with O_3 is negligible under these experimental conditions,[65] which was confirmed by conducting experiments in N_2-purged solutions to limit O_3 formation (Figure S3). Nitrobenzene is considered to be highly selective for $^{\bullet}OH$

DOI: 10.1021/acs.est.8b07225
Environ. Sci. Technol. 2019, 53, 4450−4459

compared to RCS,[22,32,33,44] although there are no published rate constants for its reaction with Cl• or $Cl_2^{-\bullet}$.[20,32,44] In contrast, benzoate reacts with •OH, Cl•, and $Cl_2^{-\bullet}$,[33] and has been used in multiple kinetic modeling studies.[22,29,33,40,46] There is debate about whether its RCS-mediated degradation is dominated by Cl• or $Cl_2^{-\bullet}$,[22,29,33,46] with one kinetic modeling study suggesting reaction with RCS is negligible.[33] We conducted a series of experiments to validate the selectivity of nitrobenzene and to identify which reactive species are responsible for benzoate degradation under our experimental conditions. These experiments are described in detail in Section S3 and summarized here.

In order to test the selectivity of nitrobenzene for •OH, we conducted experiments under highly acidic conditions where Cl_2 is the primary chlorine species (Figure 2a). This approach

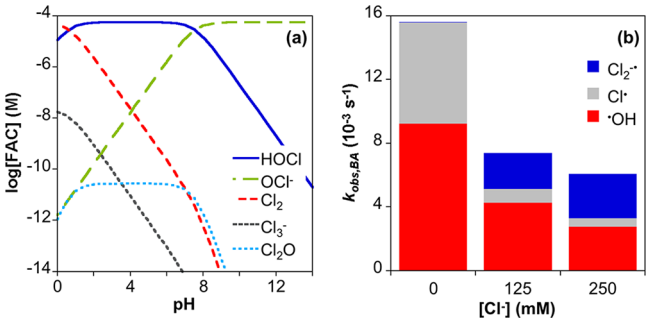

Figure 2. (a) Chlorine speciation as a function of pH for 4 mg-Cl_2/L total chlorine and 75 mg/L chloride calculated using equilibrium constants from reference 66. (b) Contribution of •OH, Cl•, and $Cl_2^{-\bullet}$ to benzoate loss as a function of chloride concentration at 254 nm (4 mg-Cl_2/L, pH 6).

has been used to assess the reactivity of organic compounds with RCS since photolysis of Cl_2 is considered to be a clean source of Cl•/$Cl_2^{-\bullet}$.[44] Contrary to previous studies that observed no nitrobenzene degradation at pH 1 (254 nm; 4−16 mg-Cl_2/L),[32,44] nitrobenzene loss was observed when 4 mg-Cl_2/L was irradiated at 254 nm at pH 0.25 (Figure S4), suggesting that nitrobenzene reacts with Cl• or $Cl_2^{-\bullet}$. However, further investigation of chlorine speciation shows that 0.71 mg-Cl_2/L HOCl is present in 4 mg-Cl_2/L total chlorine at pH 0.25 (Figure 2a) and additional experiments demonstrate that this concentration is capable of producing •OH responsible for ∼90% of the observed nitrobenzene loss (Figure S5). The remaining •OH production may be attributable to •OH formed via reaction of Cl• with H_2O (Reactions 57 and 146). Thus, these results confirm the selectivity of nitrobenzene for •OH and demonstrate that low pH conditions are not appropriate for generating Cl•/$Cl_2^{-\bullet}$ in the absence of •OH.

A series of experiments were used to identify which species are responsible for benzoate degradation under our experimental conditions. First, competition kinetics with nitrobenzene was used to evaluate the reactivity of benzoate toward RCS at pH 6 under 365 nm irradiation. The degradation of benzoate could not be explained by measured $[^\bullet OH]_{ss}$ alone (Figure S7), indicating that RCS also contribute to benzoate degradation. The effect of carbon-centered radicals on benzoate degradation is beyond the scope of this study and was not considered. In order to identify whether Cl•, $Cl_2^{-\bullet}$, or ClO• contribute to benzoate loss, experiments with varied chloride and chlorine concentrations were conducted to produce conditions that favor $Cl_2^{-\bullet}$ and ClO•, respectively.[22,29,37,40,44,46] Elevated chloride shifts the Cl•/$Cl_2^{-\bullet}$ equilibria toward $Cl_2^{-\bullet}$, while increased chlorine concentrations result in higher production of ClO• due to quenching of •OH and Cl• by both chlorine species (Reactions 29, 37, 54,[67] and 55[67,68]). Benzoate reactivity decreased under conditions that favor ClO• during chlorine variation experiments (Figure S8), demonstrating that reaction with ClO• is negligible, as expected based on the slow reaction rate (3.0×10^6 M^{-1} s^{-1}).[38] Similarly, the degradation rate of benzoate decreased with $[Cl^-]$ (Figure 2b; Figure S9), suggesting that reaction with $Cl_2^{-\bullet}$ is less important than Cl•.

The limited contribution of $Cl_2^{-\bullet}$ in the absence of added chloride was further confirmed by calculating Cl• and $Cl_2^{-\bullet}$ steady-state concentrations using a system of equations that combines measured $[Cl^-]$ and experimentally determined $[^\bullet OH]_{ss}$ with Cl•/$Cl_2^{-\bullet}$ equilibria (Section S3). For example, $Cl_2^{-\bullet}$ is responsible for 0.1% of benzoate loss with no added chloride and 30.8% with 125 mM added chloride at pH 6 (Figure 2b). Collectively, the results indicate that benzoate can be used to quantify Cl• after considering oxidation by •OH in conditions with low $[Cl^-]$. Furthermore, the system of equations approach can be used to quantitatively distinguish between •OH, Cl•, and $Cl_2^{-\bullet}$ under other experimental conditions.

Trends in Reactive Oxidant Production. In order to identify optimum conditions for chlorine photolysis as an AOP and to consider its application using light within the solar spectrum, it is critical to quantify the effect of solution conditions on reactive oxidant production. Using the probes validated in this study, we quantified steady-state concentrations of •OH and Cl• and cumulative ozone concentrations as a function of pH and wavelength because these parameters influence chlorine speciation, molar absorptivity, and quantum yields (Scheme 1).[33,34,69] Experimentally determined concentrations are presented in Figure 1, while fluence- and chlorine loss-normalized data are shown in Figures S12 and S13.

Experimental •OH steady-state concentrations decreased with increasing pH under all three irradiation wavelengths (Figure 1b). The observation of elevated $[^\bullet OH]_{ss}$ under acidic conditions agrees with previous measurements under UV-C irradiation,[32,33,40,60] while pH trends using UV-B and UV-A light have not been previously reported. $[^\bullet OH]_{ss}$ ranged from 6.2×10^{-13} to 2.1×10^{-12} M at 254 and 311 nm (Figure 1b), which is within the literature range of 10^{-14} to 10^{-12} M quantified using similar nitrobenzene concentrations (254 nm, 4−10 mg-Cl_2/L).[33,70] While $[^\bullet OH]_{ss}$ was higher under acidic conditions using 254 nm irradiation compared to 311 nm, this effect is reversed when the data are normalized by fluence or chlorine loss (Figures S12 and S13). $[^\bullet OH]_{ss}$ was a factor of 4−10 lower at 365 nm compared to 254 and 311 nm irradiation on an absolute basis (i.e., 6.0×10^{-14} to 1.9×10^{-13} M) and 20−200 times lower on a fluence-normalized basis. $[^\bullet OH]_{ss}$ at 365 nm are similar to a steady-state concentration of 3×10^{-14} M measured under simulated sunlight.[28] Note that the $[^\bullet OH]_{ss}$ experienced by contaminants in a chlorine photolysis system may be up to 10−20% higher than the values reported here due to scavenging by nitrobenzene depending on the presence of other constituents.

The impact of pH on $[^\bullet OH]_{ss}$ is partially attributable to differences in the quantum yields and reaction mechanisms of HOCl and OCl^- (Scheme 1). Although the OCl^- molar absorptivity is higher than that of HOCl at wavelengths >254

DOI: 10.1021/acs.est.8b07225
Environ. Sci. Technol. 2019, 53, 4450−4459

nm (Figure S1), the HOCl quantum yield is higher than that of OCl^- at each wavelength in this study (Scheme 1). While the decrease in $^{\bullet}OH$ production with increasing pH at 254 nm is often solely attributed to the lower quantum yield of OCl^-,[33,46] it is important to note that the reaction mechanisms of HOCl and OCl^- are also different. HOCl undergoes homolytic cleavage to form $^{\bullet}OH$ and $Cl^{\bullet}$ with reported quantum yields ranging from 0.6−1.4.[32,33] The quantum yield of HOCl at 365 nm is unknown but is hypothesized to be similar to 311 nm. In contrast, OCl^- undergoes photolysis via three separate reactions that each generate different reactive species: $O^{-\bullet}$ reacts with water to form $^{\bullet}OH$, $O(^1D)$ reacts with water to form two $^{\bullet}OH$, and $O(^3P)$ reacts with oxygen to form O_3.[34] There is less variability in the reported quantum yields of OCl^- photolysis. For example, the recently reported quantum yield of 0.55 for $^{\bullet}OH$ production by OCl^- at 254 nm[33] is nearly identical to the quantum yield of 0.544 calculated from the earlier reported quantum yields of two OCl^- photolysis pathways (Reaction 2 + 2 × Reaction 3).[34] Thus, the quantum yield of HOCl is 1.1−2.6 times higher than the quantum yield of OCl^- at 254 nm, which does not fully explain the 5.2 times higher $[^{\bullet}OH]_{ss}$ quantified at pH 6 compared to pH 10.

Preferential scavenging of $^{\bullet}OH$ by OCl^- compared to HOCl also contributes to the decrease in $[^{\bullet}OH]_{ss}$ at high pH, regardless of irradiation wavelength. The reaction of $^{\bullet}OH$ with HOCl and OCl^- is critical because, in addition to serving as a major sink of $^{\bullet}OH$, the product of the reaction (i.e., $ClO^{\bullet}$; Reactions 29 and 37 in Table S2) may be responsible for the degradation of organic compounds at high pH.[22,33,47,71] However, there is uncertainty in the rate constants; literature values vary from 8.5×10^4 to 2.0×10^9 M^{-1} s^{-1} for the reaction of $^{\bullet}OH$ and HOCl, and 8.8×10^8 to 9.8×10^9 M^{-1} s^{-1} for the reaction of $^{\bullet}OH$ and OCl^-.[10,32,33,44,72−75] We used pulse radiolysis to directly determine the absolute second-order rate constants between these chlorine species and $^{\bullet}OH$, and found values of $(1.21 \pm 0.17) \times 10^9$ and $(6.37 \pm 0.06) \times 10^9$ M^{-1} s^{-1} for HOCl and OCl^-, respectively. These rate constants are faster than those measured by gamma radiolysis[33] and those calculated using quantum mechanical models[76] but confirm the higher reactivity of $^{\bullet}OH$ with OCl^- reported previously. Pulse radiolysis measures the rate constant directly while gamma radiolysis measures the product of a reaction sequence, adding additional error to the measurement. Quantum mechanical modeling relies on assumptions (e.g., the number of hydrating water molecules) that can alter the analysis.[76]

Production and Reactivity of $Cl^{\bullet}$. The trends in experimental $Cl^{\bullet}$ steady-state concentrations with pH and wavelength were similar to the trends observed with $^{\bullet}OH$. $[Cl^{\bullet}]_{ss}$ was generally an order of magnitude lower than $[^{\bullet}OH]_{ss}$, ranging from 3.1×10^{-14} to 4.5×10^{-13} M at 254 and 311 nm and from 2.9×10^{-15} to 1.3×10^{-13} M at 365 nm (Figure 1c). Similar $[Cl^{\bullet}]_{ss}$ of $(0.4−6.3) \times 10^{-14}$ M were reported at 254 nm (pH 7).[29,77] There is some scatter with the pH trends due to error introduced by subtracting $k_{obs,NB}$ from $k_{BA,obs}$ as this two-probe method for $^{\bullet}OH$, $Cl^{\bullet}$, and $Cl_2^{-\bullet}$ is most accurate at relatively high $[Cl^{\bullet}]_{ss}$ and/or $[Cl_2^{-\bullet}]_{ss}$ (Section S3). Despite this limitation, $[Cl^{\bullet}]_{ss}$ decreases with pH at all three irradiation wavelengths. Experimental steady-state concentrations of $Cl^{\bullet}$ have not been previously reported as a function of pH at any wavelength, but kinetic models predict that $Cl^{\bullet}$ will decrease with increasing pH at 254 nm.[33,46] As with $^{\bullet}OH$, $[Cl^{\bullet}]_{ss}$ is higher at both 254 and 311 nm than 365 nm when normalized by fluence or chlorine loss across all pH values (Figures S12 and S13).

The quantum yields of HOCl and OCl^- photolysis, as well as their relative reaction rates with $Cl^{\bullet}$, result in the observed trends in $[Cl^{\bullet}]_{ss}$. The quantum yield of $Cl^{\bullet}$ from HOCl is identical to the $^{\bullet}OH$ quantum yield because HOCl undergoes homolytic cleavage to form the two radicals.[34] However, only one of the three OCl^- photolysis pathways produces $Cl^{\bullet}$ (Reaction 2), which emphasizes the importance of considering the three pathways of OCl^- photolysis separately. Thus, the quantum yield of $Cl^{\bullet}$ from OCl^- is 1.95 and 1.31 times lower than the quantum yield of $^{\bullet}OH$ at 254 and 311 nm, respectively, while the quantum yields of $^{\bullet}OH$ and $Cl^{\bullet}$ are identical at 365 nm because Reaction 3 is negligible (Scheme 1). In addition, OCl^- reacts with $Cl^{\bullet}$ 2.75 times more quickly than HOCl (Reactions 54 and 55). Collectively, these factors result in the observed decrease in $[Cl^{\bullet}]_{ss}$ with increasing pH for both 254 and 365 nm (Figure 1c). There is no pH trend for $[Cl^{\bullet}]_{ss}$ at 311 nm, likely because OCl^- absorbs more light than HOCl, so the difference in quantum yield is matched by the difference in molar absorptivity (Scheme 1; Figure S2).

Ozone Generation. Although O_3 has not previously been measured at wavelengths less than 320 nm,[20,22,33,47,71,73] we observe the formation of O_3 at all three irradiation wavelengths (Figure 1d). Cumulative O_3 concentrations were determined by the maximum production of benzaldehyde over the course of the experiment and were greatest at 254 nm (0.9−2.2 μM), followed by 365 nm (0.8−1.3 μM) and 311 nm (0.4−1.1 μM). These concentrations are similar to the 1.8 μM cumulative O_3 measured during sunlight irradiation of 8 mg-Cl_2/L.[28] These concentrations are low relative to the concentration of O_3 used as a primary oxidant (e.g., ∼1 mg/L)[48] in drinking water treatment, but O_3 is still an important oxidant. Previous studies at sunlight wavelengths demonstrate that O_3 generated during chlorine photolysis contributes to organic compound degradation[78] and pathogen inactivation.[28]

The cumulative concentration of ozone generally increases with increasing pH because $O(^3P)$, the precursor to ozone generation, is only formed during the photolysis of OCl^- (Reaction 4). This trend is observed until pH 8 where O_3 concentration peaks at all three wavelengths (Figure 1d), suggesting an optimum condition for the formation of ozone. The final decrease at high pH may be attributable to scavenging of O_3 by OCl^- (Reactions 84 and 85). The higher concentration of O_3 at 254 nm is unexpected based on the known quantum yields (Scheme 1) and may be partially attributable to the higher molar absorptivity of OCl^- at 254 nm relative to 365 nm. Although the difference between cumulative O_3 at 254 and 311 nm cannot be explained by molar absorptivity or quantum yield, the cumulative ozone concentrations at each wavelength are on the same order of magnitude in absolute terms (Figure 1d) and are equivalent when fluence-normalized (Figure S12d).

Demonstration of O_3 formation during chlorine photolysis at 254 nm is a novel finding that changes the analysis of previous research. The increased degradation of organic compounds at high pH is typically attributed to reaction with $ClO^{\bullet}$ based on quenching by *t*-butanol and the high $[ClO^{\bullet}]_{ss}$ predicted by kinetic models (∼10^{-9} M).[14,22,23,33,37,47,71] For example, the degradation of trimethoprim, carbamazepine, and microcystin-LR at high pH was attributed to reaction with $ClO^{\bullet}$.[14,40,47] However, these compounds also react relatively quickly with O_3 (k = (0.5−

DOI: 10.1021/acs.est.8b07225
Environ. Sci. Technol. 2019, 53, 4450−4459

7.4) × 10^4, 3 × 10^5, and 3.8 × 10^4 M^{-1} s^{-1}, respectively) and O_3 has not been included in kinetic models.[48,49,79,80] Furthermore, it is important to note that *t*-butanol is also a quencher for $O(^3P)$ (i.e., the O_3 precursor; Reaction 9).[79,81] Thus, we propose that enhanced oxidation of compounds at high pH may be partially attributable to reaction with O_3 due to the direct evidence of O_3 formation over a wide range of irradiation conditions.

Comparison of Kinetic Models. Kinetic modeling is an important component of studying chlorine photolysis because the number of reactive species makes quenching and probe studies incomplete. Kinetic models that describe chlorine photolysis under UV-C irradiation range in complexity (25−78 reactions; Table S4) and are used to predict chlorine loss rates and reactive oxidant steady-state concentrations, as well as to optimize treatment systems.[22,29,33,40,46] While some models are validated against a limited number of experimental results,[22,33] models are frequently extrapolated to other conditions or contaminants without further validation and some are not compared directly to experimental measurements made in the same study (e.g., measured $[^{\bullet}OH]_{ss}$ or estimated contaminant loss due to $ClO^{\bullet}$).[22,37,40] Furthermore, it is impossible to validate steady-state concentrations of reactive species for which there are no selective probes (e.g., $ClO^{\bullet}$). Finally, existing models do not incorporate the formation of O_3 as one of the relevant oxidant species. To address these gaps, we built a kinetic model containing 196 reactions by expanding the previous models to include the reactions of O_3 and additional radical−radical reactions that were discovered during a comprehensive literature search (Table S2).

The five previously published models were reconstructed in Kintecus and compared to the expanded model built in this study, along with the experimental data. Comparison between models is limited to 254 nm irradiation because all past work focused on this wavelength, while discussion of modeling efforts at 311 and 365 nm is below. The literature models were all run using the same chlorine photolysis rates, which were calculated based on the measured sample absorbance at each pH value and literature quantum yields (Section S5), in order to compare the accuracy of models based on their elementary reactions. The modeled results were compared to the experimental measurements of chlorine loss, $[^{\bullet}OH]_{ss}$, $[Cl^{\bullet}]_{ss}$, and cumulative O_3 concentrations by calculating root-mean-square error (Table S6).

The side-by-side comparison of existing models that were constructed to model highly similar conditions reveals that there is little agreement across the models for chlorine loss and the considered oxidants. There is wide variability in the predicted trends of chlorine loss, with some models (e.g., Sun et al., 2017 and Guo et al., 2017) showing a strong pH dependence that does not match the experimental results or the trends observed by the other four models (Figure 3a). It is worth noting that the model that most accurately describes chlorine loss (Chuang et al., 2017) was developed for this specific parameter.[33] All six considered models report that $[^{\bullet}OH]_{ss}$ decreases with increasing pH, in agreement with experimental observations (Figure 3b). However, the magnitude of predicted $[^{\bullet}OH]_{ss}$ ranges widely (e.g., from 1.0 × 10^{-14} to 2.6 × 10^{-12} M at pH 6). Similar results are observed for $Cl^{\bullet}$ (Figure S14a), although both the Chuang et al., 2017 and Li et al., 2017 models predict $[Cl^{\bullet}]_{ss}$ that are 1−2 orders of magnitude lower than the other models and the experimental data. This could explain why Chuang et al., 2017 estimated

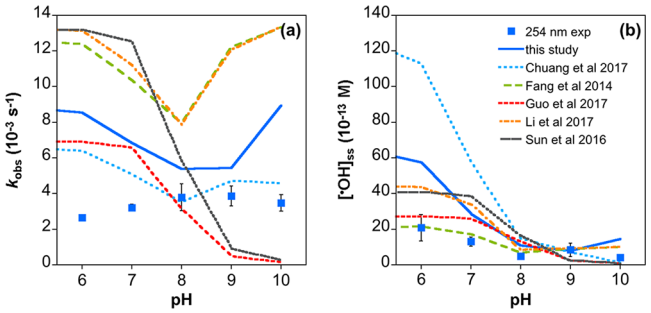

Figure 3. Comparison of experimental data with model output from the model developed in this study along with literature models[22,29,33,40,46] for the (a) observed free chlorine loss rate constants and (b) hydroxyl radical steady-state concentrations as a function of pH during irradiation of 4 mg-Cl_2/L at 254 nm.

that 80% of benzoate reactivity was due to $^{\bullet}OH$, while experimental observations show that $Cl^{\bullet}$ is responsible for ∼40% of benzoate loss (Figure 2b). As expected, the five previously published models did not predict any ozone formation, while our model underpredicted cumulative ozone generation by 0−4 orders of magnitude (Figure S14b).

There is no single model that predicts all four parameters considered in our comparison. For example, the model that most accurately predicts chlorine loss rate constant (Chuang et al., 2017) overpredicts $[^{\bullet}OH]_{ss}$ and underpredicts $[Cl^{\bullet}]_{ss}$ (Figures 3b and S14a). Similarly, the model that accurately predicts both $[^{\bullet}OH]_{ss}$ and $[Cl^{\bullet}]_{ss}$ (Fang et al., 2014) is one of the least accurate in predicting chlorine loss. The model developed in this study generally predicts the order of magnitude and trends in chlorine loss, $[^{\bullet}OH]_{ss}$, and $[Cl^{\bullet}]_{ss}$ but is never the most, or least, accurate.

The differences in model output result from the sets of reactions included in each model. For example, modeled $[^{\bullet}OH]_{ss}$ varies by 2 orders of magnitude when the models are run with the same direct photolysis rates and quantum yields (Table S5). Surprisingly, the Fang et al., 2014 model[46] is the most accurate at predicting $[^{\bullet}OH]_{ss}$ even though it is the most simplistic model (Table S4), with very few reactions describing $^{\bullet}OH$ reactivity. In contrast, the two models with the most reactions, this study and Chuang et al., 2017, are the worst predictors of $[^{\bullet}OH]_{ss}$ (Table S6).[33] These discrepancies are representative across parameters, where changes in the number of reactions describing a compound impact its formation and loss. While there are many missing rate constants that need to be filled in for all reactive oxidants (e.g., reactions between oxidants and buffers), the side-by-side model comparison suggests that simply adding additional reactions does not improve model accuracy. There are also differences in the rate constants used for some reactions, but these values generally differ by less than an order of magnitude and are for minor reactions that are unlikely to impact the model.

The loss of chlorine and production of oxidants was also modeled at 311 and 365 nm using measured absorbance, literature quantum yields (Scheme 1), and known kinetic reactions (Table S2). The 311 nm model results in the most accurate predictions of O_3 production and accurately predicts the observed loss rate of chlorine and $[Cl^{\bullet}]_{ss}$ (Figure S15). However, the model overpredicts $[^{\bullet}OH]_{ss}$ by more than an order of magnitude at high pH, which may be the result of the high molar absorptivity of OCl^- and correspondingly high expected production of $^{\bullet}OH$. While the 311 nm model was

DOI: 10.1021/acs.est.8b07225
Environ. Sci. Technol. 2019, 53, 4450−4459

successful for three of the considered parameters, the 365 nm kinetic model was less accurate for all parameters (Figure S16). For example, the 365 nm model overpredicts chlorine loss rate constants and $[^{\bullet}OH]_{ss}$, while underpredicting O_3 formation. This model is based on an assumed quantum yield of 1.0 for HOCl because a literature value is not available, which likely introduces uncertainty to the model. Although there are no existing kinetic models available for comparison at the higher wavelengths, the overall accuracy of these models is similar to that of the revised 254 nm model.

The wide variety of model results suggests that a comprehensive model for chlorine photolysis based on a first-principles approach is not yet possible. The addition of >100 reactions to previously published models resulted in a model that is moderately good at predicting the formation of oxidants by chlorine photolysis relative to others. However, it is still not the best model for any of the parameters. It is possible that additional elementary reactions could further improve this model, but we may never have all of the necessary rate constants to accurately determine the formation of oxidants in this system due to the number of radicals and subsequent chain reactions. Due to the challenges in predicting the production of reactive oxidants that can be compared to experimental data, it is unlikely that models can accurately determine the formation of other oxidant species that cannot yet be validated experimentally, such as $ClO^{\bullet}$. Additionally, the variability between models suggests that using models to attribute reactivity toward a given organic compound may not be accurate, as seen with the modeled difference in benzoate reactivity toward $Cl^{\bullet}$ and $^{\bullet}OH$.[33,46]

Implications for Water Treatment. Understanding the formation of reactive oxidants during chlorine photolysis is essential to future applications of advanced oxidation or disinfection.[71,82−85] Chlorine photolysis produces a suite of reactive oxidants, including $^{\bullet}OH$, $Cl^{\bullet}$, and O_3 that are capable of degrading organic contaminants. $^{\bullet}OH$ and $Cl^{\bullet}$ steady-state concentrations are greater under acidic conditions using 254 or 311 nm irradiation, while O_3 is generally greatest at high pH using 254 nm irradiation (Figure 1). $Cl^{\bullet}$ and $Cl_2^{-\bullet}$ may be problematic because they can react via chlorine addition to form chlorinated disinfection byproducts.[37,40−42] Both O_3 and $^{\bullet}OH$ are optimized during treatment at 254 nm, though at opposite ends of the pH spectrum. The fluence- and chlorine loss-normalized oxidant concentrations provide additional insight into this system. If treatment is chlorine limited, 254 nm is the optimum irradiation wavelength because it produces the most $^{\bullet}OH$ per chlorine molecule degraded (Figure S13). If energy consumption is the primary concern, 311 nm will optimize the production of $^{\bullet}OH$ for each photon produced (Figure S12). These results agree with previous observations of chlorine loss rates and $[^{\bullet}OH]_{ss}$ at $\lambda < 301$ nm.[60] Although both 254 and 311 nm irradiation wavelengths are more efficient in producing oxidants than 365 nm, the chlorine loss rate constants and oxidant concentrations at 365 nm are on the same order of magnitude as the other wavelengths when normalized by either fluence or chlorine loss.

O_3 is a powerful oxidant that has been largely overlooked in previous studies. Experimentally determined cumulative ozone concentrations demonstrate that this oxidant is present under all studied conditions, albeit at lower concentrations than are typically used in drinking water treatment. As O_3 reacts with many organic compounds,[48,82,85,86] further investigation into its role in contaminant degradation during chlorine photolysis is needed. The formation of O_3 is also crucial because it results in bromate formation in bromine-containing waters.[48,87−89]

Finally, this study suggests that chlorine photolysis has potential in solar treatment applications. Although 254 nm is the most effective wavelength at producing $^{\bullet}OH$, both 311 and 365 nm irradiation result in oxidant generation. Thus, chlorine photolysis is unique among light-based AOPs as it could be applied in regions without access to conventional drinking water treatment for point-of-use solar water disinfection.[20,30,71,82−85] For example, degradation of DEET, caffeine, and carbamazepine and enhanced inactivation of *Cryptosporidium parvum* have been observed when chlorine undergoes photolysis by solar light.[29,30,79,81] Our work provides insight into the mechanism of oxidant production under these conditions and suggests that $^{\bullet}OH$ and O_3 may contribute to previously observed contaminant removal.

■ ASSOCIATED CONTENT

Supporting Information

The Supporting Information is available free of charge on the ACS Publications website at DOI: 10.1021/acs.est.8b07225.

Analytical methods, probe validation, comprehensive kinetic model comparison, rate constant measurements, and fluence- and chlorine loss-normalized reactive oxidant production (PDF)

Kinetic model (XLSX)

■ AUTHOR INFORMATION

Corresponding Author

*E-mail: remucal@wisc.edu. Phone: (608) 262-1820. Fax: (608) 262-0454.

ORCID

Devon Manley Bulman: 0000-0002-4999-9367

Christina K. Remucal: 0000-0003-4285-7638

Notes

The authors declare no competing financial interest.

■ ACKNOWLEDGMENTS

This work was supported by an NSF CAREER award (CBET-1451932) and a National Water Research Institute Graduate Research Fellowship (awarded to D.M.B.)

■ REFERENCES

(1) Benotti, M. J.; Trenholm, R. A.; Vanderford, B. J.; Holady, J. C.; Stanford, B. D.; Snyder, S. A. Pharmaceuticals and endocrine disrupting compounds in U.S. drinking water. *Environ. Sci. Technol.* **2009**, *43* (3), 597−603.

(2) Fairbairn, D. J.; Arnold, W. A.; Barber, B. L.; Kaufenberg, E. F.; Koskinen, W. C.; Novak, P. J.; Rice, P. J.; Swackhamer, D. L. Contaminants of emerging concern: Mass balance and comparison of wastewater effluent and upstream sources in a mixed-use watershed. *Environ. Sci. Technol.* **2016**, *50* (1), 36−45.

(3) Kolpin, D. W.; Furlong, E. T.; Meyer, M. T.; Thurman, E. M.; Zaugg, S. D.; Barber, L. B.; Buxton, H. T. Pharmaceuticals, hormones, and other organic wastewater contaminants in U.S. streams, 1999−2000: A national reconnaissance. *Environ. Sci. Technol.* **2002**, *36* (6), 1202−1211.

(4) Kostich, M. S.; Batt, A. L.; Lazorchak, J. M. Concentrations of prioritized pharmaceuticals in effluents from 50 large wastewater treatment plants in the U.S. and implications for risk estimation. *Environ. Pollut.* **2014**, *184*, 354−359.

(5) Stackelberg, P. E.; Furlong, E. T.; Meyer, M. T.; Zaugg, S. D.; Henderson, A. K.; Reissman, D. B. Persistence of pharmaceutical

DOI: 10.1021/acs.est.8b07225
Environ. Sci. Technol. 2019, 53, 4450−4459

compounds and other organic wastewater contaminants in a conventional drinking-water-treatment plant. *Sci. Total Environ.* **2004**, *329* (1−3), 99−113.
(6) Mompelat, S.; Le Bot, B.; Thomas, O. Occurrence and fate of pharmaceutical products and by-products, from resource to drinking water. *Environ. Int.* **2009**, *35* (5), 803−814.
(7) Masoner, J. R.; Kolpin, D. W.; Furlong, E. T.; Cozzarelli, I. M.; Gray, J. L. Landfill leachate as a mirror of today's disposable society: Pharmaceuticals and other contaminants of emerging concern in final leachate from landfills in the conterminous united states. *Environ. Toxicol. Chem.* **2016**, *35* (4), 906−918.
(8) Gray, J. L.; Borch, T.; Furlong, E. T.; Davis, J. G.; Yager, T. J.; Yang, Y. Y.; Kolpin, D. W. Rainfall-runoff of anthropogenic waste indicators from agricultural fields applied with municipal biosolids. *Sci. Total Environ.* **2017**, *580*, 83−89.
(9) Richardson, S. D.; Ternes, T. A. Water analysis: Emerging contaminants and current issues. *Anal. Chem.* **2011**, *83* (12), 4614−4648.
(10) Buxton, G. V.; Greenstock, C. L.; Helman, W. P.; Ross, A. B. Critical review of rate constants for reactions of hydrated electrons, hydrogen atoms and hydroxyl radicals (OH/O^-) in aqueous solution. *J. Phys. Chem. Ref. Data* **1988**, *17* (2), 513−886.
(11) Buxton, G. V.; Bydder, M.; Salmon, G. A.; Williams, J. E. The reactivity of chlorine atoms in aqueous solution Part III. The reactions of Cl with solutes. *Phys. Chem. Chem. Phys.* **2000**, *2*, 237−245.
(12) An, T.; Yang, H.; Li, G.; Song, W.; Cooper, W. J.; Nie, X. Kinetics and mechanism of advanced oxidation processes (AOPs) in degradation of ciprofloxacin in water. *Appl. Catal., B* **2010**, *94* (3−4), 288−294.
(13) Cai, M.; Sun, P.; Zhang, L.; Huang, C. H. UV/peracetic acid for degradation of pharmaceuticals and reactive species evaluation. *Environ. Sci. Technol.* **2017**, *51* (24), 14217−14224.
(14) Duan, X.; Sanan, T.; De La Cruz, A.; He, X.; Kong, M.; Dionysiou, D. D. Susceptibility of the algal toxin microcystin-LR to UV/chlorine process: Comparison with chlorination. *Environ. Sci. Technol.* **2018**, *52* (15), 8252−8262.
(15) García Einschlag, F. S.; Carlos, L.; Capparelli, A. L. Competition kinetics using the UV/H_2O_2 process: A structure reactivity correlation for the rate constants of hydroxyl radicals toward nitroaromatic compounds. *Chemosphere* **2003**, *53* (1), 1−7.
(16) Huang, Y.; Liu, Y.; Kong, M.; Xu, E. G.; Coffin, S.; Schlenk, D.; Dionysiou, D. D. Efficient degradation of cytotoxic contaminants of emerging concern by UV/H_2O_2. *Environ. Sci.: Water Res. Technol.* **2018**, *4* (9), 1272−1281.
(17) Khan, S. J.; Gagnon, G. A.; Templeton, M. R.; Dionysiou, D. D. The rapidly growing role of UV-AOPs in the production of safe drinking water. *Environ. Sci.: Water Res. Technol.* **2018**, *4* (9), 1211−1212.
(18) Lee, Y.; Gerrity, D.; Lee, M.; Gamage, S.; Pisarenko, A.; Trenholm, R. A.; Canonica, S.; Snyder, S. A.; von Gunten, U. Organic contaminant abatement in reclaimed water by UV/H_2O_2 and a combined process consisting of O_3/H_2O_2 followed by UV/H_2O_2: Prediction of abatement efficiency, energy consumption, and byproduct formation. *Environ. Sci. Technol.* **2016**, *50* (7), 3809−3819.
(19) Bossmann, S. H.; Oliveros, E.; Göb, S.; Siegwart, S.; Dahlen, E. P.; Payawan, L.; Straub, M.; Wörner, M.; Braun, A. M. New evidence against hydroxyl radicals as reactive intermediates in the thermal and photochemically enhanced Fenton reactions. *J. Phys. Chem. A* **1998**, *102* (28), 5542−5550.
(20) Remucal, C. K.; Manley, D. Emerging investigators series: The efficacy of chlorine photolysis as an advanced oxidation process for drinking water treatment. *Environ. Sci.: Water Res. Technol.* **2016**, *2* (4), 565−579.
(21) Huang, W.; Bianco, A.; Brigante, M.; Mailhot, G. UVA-UVB activation of hydrogen peroxide and persulfate for advanced oxidation processes: Efficiency, mechanism and effect of various water constituents. *J. Hazard. Mater.* **2018**, *347*, 279−287.
(22) Li, W.; Jain, T.; Ishida, K.; Remucal, C. K.; Liu, H. A mechanistic understanding of the degradation of trace organic contaminants by UV/hydrogen peroxide, UV/persulfate and UV/free chlorine for water reuse. *Environ. Sci.: Water Res. Technol.* **2017**, *3* (1), 128−138.
(23) Pan, M.; Wu, Z.; Tang, C.; Guo, K.; Cao, Y.; Fang, J. Emerging investigators series: Comparative study of naproxen degradation by the UV/chlorine and the UV/H_2O_2 advanced oxidation processes. *Environ. Sci.: Water Res. Technol.* **2018**, *4* (9), 1219−1230.
(24) Pati, S. G.; Arnold, W. A. Reaction rates and product formation during advanced oxidation of ionic liquid cations by UV/peroxide, UV/persulfate, and UV/chlorine. *Environ. Sci.: Water Res. Technol.* **2018**, *4* (9), 1310−1320.
(25) Chu, W.; Gao, N.; Yin, D.; Krasner, S. W.; Mitch, W. A. Impact of UV/H_2O_2 pre-oxidation on the formation of haloacetamides and other nitrogenous disinfection byproducts during chlorination. *Environ. Sci. Technol.* **2014**, *48* (20), 12190−12198.
(26) Morgan, M. S.; Van Trieste, P. F.; Garlick, S. M.; Mahon, M. J.; Smith, A. L. Ultraviolet molar absorptivities of aqueous hydrogen peroxide and hydroperoxyl ion. *Anal. Chim. Acta* **1988**, *215*, 325−329.
(27) Buck, R. P.; Singhadeja, S.; Rogers, L. B. Ultraviolet absorption spectra of some inorganic ions in aqueous solutions. *Anal. Chem.* **1954**, *26* (7), 1240−1242.
(28) Forsyth, J. E.; Zhou, P.; Mao, Q.; Asato, S. S.; Meschke, J. S.; Dodd, M. C. Enhanced inactivation of bacillus subtilis spores during solar photolysis of free available chlorine. *Environ. Sci. Technol.* **2013**, *47* (22), 12976−12984.
(29) Sun, P.; Lee, W. N.; Zhang, R.; Huang, C. H. Degradation of DEET and caffeine under UV/chlorine and simulated sunlight/chlorine conditions. *Environ. Sci. Technol.* **2016**, *50* (24), 13265−13273.
(30) Young, T. R.; Li, W.; Guo, A.; Korshin, G. V.; Dodd, M. C. Characterization of disinfection byproduct formation and associated changes to dissolved organic matter during solar photolysis of free available chlorine. *Water Res.* **2018**, *146*, 318−327.
(31) Yin, R.; Zhong, Z.; Ling, L.; Shang, C. The fate of dichloroacetonitrile in UV/Cl_2 and UV/H_2O_2 processes: Implications on potable water reuse. *Environ. Sci.: Water Res. Technol.* **2018**, *4* (9), 1295−1302.
(32) Watts, M. J.; Linden, K. G. Chlorine photolysis and subsequent OH radical production during UV treatment of chlorinated water. *Water Res.* **2007**, *41* (13), 2871−2878.
(33) Chuang, Y. H.; Chen, S.; Chinn, C. J.; Mitch, W. A. Comparing the UV/monochloramine and UV/free chlorine advanced oxidation processes (AOPs) to the UV/hydrogen peroxide AOP under scenarios relevant to potable reuse. *Environ. Sci. Technol.* **2017**, *51* (23), 13859−13868.
(34) Buxton, G. V.; Subhani, M. S. Radiation chemistry and photochemistry of oxychlorine ions Part 2. Photodecomposition of aqueous solutions of hypochlorite ions. *J. Chem. Soc., Faraday Trans. 1* **1972**, *68*, 958−969.
(35) Gilbert, B. C.; Stell, J. K.; Peet, W. J.; Radford, K. J. Generation and reactions of the chlorine atom in aqueous solution. *J. Chem. Soc., Faraday Trans. 1* **1988**, *84* (10), 3319−3330.
(36) Zhang, K.; Parker, K. M. Halogen radical oxidants in natural and engineered aquatic systems. *Environ. Sci. Technol.* **2018**, *52* (17), 9579−9594.
(37) Wu, Z.; Guo, K.; Fang, J.; Yang, X.; Xiao, H.; Hou, S.; Kong, X.; Shang, C.; Yang, X.; Meng, F.; Chen, L. Factors affecting the roles of reactive species in the degradation of micropollutants by the UV/chlorine process. *Water Res.* **2017**, *126*, 351−360.
(38) Alfassi, Z. B.; Huie, R. E.; Mosseri, S.; Neta, P. Kinetics of one-electron oxidation by the ClO radical. *Radiat. Phys. Chem.* **1988**, *32* (1), 85−88.
(39) Hasegawa, K.; Neta, P. Rate constants and mechanisms of reaction of chloride (Cl_2^-) radicals. *J. Phys. Chem.* **1978**, *82* (8), 854−857.
(40) Guo, K.; Wu, Z.; Shang, C.; Yao, B.; Hou, S.; Yang, X.; Song, W.; Fang, J. Radical chemistry and structural relationships of PPCP degradation by UV/chlorine treatment in simulated drinking water. *Environ. Sci. Technol.* **2017**, *51* (18), 10431−10439.

DOI: 10.1021/acs.est.8b07225
Environ. Sci. Technol. 2019, 53, 4450−4459

(41) Yang, Y.; Pignatello, J. J. Participation of the halogens in photochemical reactions in natural and treated waters. *Molecules* **2017**, *22* (10), 1684.
(42) Liu, W.; Cheung, L.-M.; Yang, X.; Shang, C. THM, HAA and CNCl formation from UV irradiation and chlor(am)ination of selected organic waters. *Water Res.* **2006**, *40* (10), 2033−2043.
(43) Molina, M. J.; Ishiwata, T.; Molina, L. T. Production of hydroxyl from photolysis of hypochlorous acid at 307−309 nm. *J. Phys. Chem.* **1980**, *84* (8), 821−826.
(44) Nowell, L. H.; Hoigné, J. Photolysis of aqueous chlorine at sunlight and ultraviolet wavelengths - II. Hydroxyl radical production. *Water Res.* **1992**, *26*, 599−605.
(45) Cheng, S.; Zhang, X.; Yang, X.; Shang, C.; Song, W.; Fang, J.; Pan, Y. The multiple role of bromide ion in PPCPs degradation under UV/chlorine treatment. *Environ. Sci. Technol.* **2018**, *52* (4), 1806−1816.
(46) Fang, J.; Fu, Y.; Shang, C. The roles of reactive species in micropollutant degradation in the UV/free chlorine system. *Environ. Sci. Technol.* **2014**, *48* (3), 1859−1868.
(47) Wu, Z.; Fang, J.; Xiang, Y.; Shang, C.; Li, X.; Meng, F.; Yang, X. Roles of reactive chlorine species in trimethoprim degradation in the UV/chlorine process: Kinetics and transformation pathways. *Water Res.* **2016**, *104*, 272−282.
(48) von Gunten, U. Ozonation of drinking water: Part I. Oxidation kinetics and product formation. *Water Res.* **2003**, *37*, 1443−1467.
(49) Kuang, J.; Huang, J.; Wang, B.; Cao, Q.; Deng, S.; Yu, G. Ozonation of trimethoprim in aqueous solution: Identification of reaction products and their toxicity. *Water Res.* **2013**, *47* (8), 2863−2872.
(50) Laszakovits, J. R.; Berg, S. M.; Anderson, B. G.; O'Brien, J. E.; Wammer, K. H.; Sharpless, C. M. *p*-Nitroanisole/pyridine and *p*-nitroacetophenone/pyridine actinometers revisited: Quantum yield in comparison to ferrioxalate. *Environ. Sci. Technol. Lett.* **2017**, *4* (1), 11−14.
(51) McConville, M. B.; Hubert, T. D.; Remucal, C. K. Direct photolysis rates and transformation pathways of the lampricides TFM and niclosamide in simulated sunlight. *Environ. Sci. Technol.* **2016**, *50* (18), 9998−10006.
(52) Maizel, A. C.; Li, J.; Remucal, C. K. Relationships between dissolved organic matter composition and photochemistry in lakes of diverse trophic status. *Environ. Sci. Technol.* **2017**, *51* (17), 9624−9632.
(53) Galbavy, E. S.; Ram, K.; Anastasio, C. 2-Nitrobenzaldehyde as a chemical actinometer for solution and ice photochemistry. *J. Photochem. Photobiol., A* **2010**, *209* (2−3), 186−192.
(54) Baeza, C.; Knappe, D. R. U. Transformation kinetics of biochemically active compounds in low-pressure UV photolysis and UV/H_2O_2 advanced oxidation processes. *Water Res.* **2011**, *45* (15), 4531−4543.
(55) Hollingsworth, C. A.; Seybold, P. G.; Hadad, C. M. Substituent effects on the electronic structure and pK_a of benzoic acid. *Int. J. Quantum Chem.* **2002**, *90* (4−5), 1396−1403.
(56) Neta, P.; Madhavan, V.; Zemel, H.; Fessenden, R. W. Rate constants and mechanism of reaction of SO_4^- with aromatic compounds. *J. Am. Chem. Soc.* **1977**, *99* (1), 163−164.
(57) Eaton, A. D.; Clesceri, L. S.; Greenberg, A. E., Eds.; *Standard Methods for the Examination of Water and Wastewater*; United Book Press, Inc.: Baltimore, 1995.
(58) Willson, V. A. Determination of available chlorine in hypochlorite solutions by direct titration with sodium thiosulfate. *Ind. Eng. Chem., Anal. Ed.* **1935**, *7* (1), 44−45.
(59) Ianni, J. C. A Comparison of the Bader-Deuflhard and the Cash-Karp Runge-Kutta Integrators for the GRI-MECH 3.0 Model Based on the Chemical Kinetics Code Kintecus. In*Computational Fluid and Solid Mechanics*; Bathe, K.J., Ed.; Elsevier: Oxford, 2003; pp1368−1372.
(60) Yin, R.; Ling, L.; Shang, C. Wavelength-dependent chlorine photolysis and subsequent radical production using UV-LEDs as light sources. *Water Res.* **2018**, *142*, 452−458.
(61) Kwon, M.; Yoon, Y.; Kim, S.; Jung, Y.; Hwang, T.-M.; Kang, J.-W. Removal of sulfamethoxazole, ibuprofen and nitrobenzene by UV and UV/chlorine processes: A comparative evaluation of 275 nm LED-UV and 254 nm LP-UV. *Sci. Total Environ.* **2018**, *637−638*, 1351−1357.
(62) Feng, Y.; Smith, D. W.; Bolton, J. R. Photolysis of aqueous free chlorine species (HOCl and OCl^-) with 254 nm ultraviolet light. *J. Environ. Eng. Sci.* **2007**, *6* (3), 277−284.
(63) Jin, J.; El-Din, M. G.; Bolton, J. R. Assessment of the UV/chlorine process as an advanced oxidation process. *Water Res.* **2011**, *45* (4), 1890−1896.
(64) Zhao, Q.; Shang, C.; Zhang, X. Effects of bromide on UV/chlorine advanced oxidation process. *Water Sci. Technol.: Water Supply* **2009**, *9* (6), 627.
(65) Hoigné, J.; Bader, H. Rate constants of reactions of ozone with organic and inorganic compounds in water—I: Non-dissociating organic compounds. *Water Res.* **1983**, *17*, 173−183.
(66) Korshin, G. V. In *Aquatic Redox Chemistry*; Tratnyek, P. G.; Grundl, T. J., Haderlein, S. B., Eds.; American Chemical Society: Washington, DC, 2011, Vol. *1071*, pp 223−245.
(67) Zehavi, D.; Rabani, J. Pulse radiolytic investigation of O_{aq}^- radical ions. *J. Phys. Chem.* **1971**, *75* (11), 1738−1744.
(68) Jayson, G. G.; Parsons, B. J.; Swallow, A. J. Some simple, highly reactive, inorganic chlorine derivatives in aqueous solution. *J. Chem. Soc., Faraday Trans. 1* **1973**, *69*, 1597−1607.
(69) Buxton, G. V.; Subhani, M. S. Radiation chemistry and photochemistry of oxychlorine ions Part 1. Radiolysis of aqueous solutions of hypochlorite and chlorite ions. *J. Chem. Soc., Faraday Trans. 1* **1972**, *68* (0), 947−957.
(70) Wang, D.; Bolton, J. R.; Hofmann, R. Medium pressure UV combined with chlorine advanced oxidation for trichloroethylene destruction in a model water. *Water Res.* **2012**, *46* (15), 4677−4686.
(71) Dodd, M. C.; Huang, C. H. Aqueous chlorination of the antibacterial agent trimethoprim: Reaction kinetics and pathways. *Water Res.* **2007**, *41* (3), 647−655.
(72) Connick, R. E. The interaction of hydrogen peroxide and hypochlorous acid in acidic solutions containing chloride ion. *J. Am. Chem. Soc.* **1947**, *69* (6), 1509−1514.
(73) Buxton, G. V.; Subhani, M. S. Radiation chemistry and photochemistry of oxychlorine ions Part 3. Photodecomposition of aqueous solutions of chloride ions. *J. Chem. Soc., Faraday Trans. 1* **1972**, *68*, 970−977.
(74) Anastasio, C.; Matthew, B. M. A chemical probe technique for the determination of reactive halogen species in aqueous solution: Part 2 Chloride solutions and mixed bromide/chloride solutions. *Atmos. Chem. Phys.* **2006**, *6*, 2439−2451.
(75) Zuo, Z.; Katsumura, Y.; Ueda, K.; Ishigure, K. Reactions between some inorganic radicals and oxychlorides studied by pulse radiolysis and laser photolysis. *J. Chem. Soc., Faraday Trans.* **1997**, *93* (10), 1885−1891.
(76) Minakata, D.; Kamath, D.; Maetzold, S. Mechanistic insight into the reactivity of chlorine-derived radicals in the aqueous-phase UV-chlorine advanced oxidation process: Quantum mechanical calculations. *Environ. Sci. Technol.* **2017**, *51* (12), 6918−6926.
(77) Varanasi, L.; Coscarelli, E.; Khaksari, M.; Mazzoleni, L. R.; Minakata, D. Transformations of dissolved organic matter induced by UV photolysis, hydroxyl radicals, chlorine radicals, and sulfate radicals in aqueous-phase UV-based advanced oxidation processes. *Water Res.* **2018**, *135*, 22−30.
(78) Hua, Z.; Guo, K.; Kong, X.; Lin, S.; Wu, Z.; Wang, L.; Huang, H.; Fang, J. PPCP degradation and DBP formation in the solar/free chlorine system: Effects of pH and dissolved oxygen. *Water Res.* **2019**, *150*, 77−85.
(79) Yang, B.; Kookana, R. S.; Williams, M.; Du, J.; Doan, H.; Kumar, A. Removal of carbamazepine in aqueous solutions through solar photolysis of free available chlorine. *Water Res.* **2016**, *100*, 413−420.

DOI: 10.1021/acs.est.8b07225
Environ. Sci. Technol. 2019, 53, 4450−4459

(80) Shawwa, A. R.; Smith, D. W.; Sego, D. C. Color and chlorinated organics removal from pulp mills wastewater using activated petroleum coke. *Water Res.* **2001**, *35* (3), 745−749.
(81) Zhou, P.; Di Giovanni, G. D.; Meschke, J. S.; Dodd, M. C. Enhanced inactivation of cryptosporidium parvum oocysts during solar photolysis of free available chlorine. *Environ. Sci. Technol. Lett.* **2014**, *1* (11), 453−458.
(82) Dodd, M. C.; Kohler, H.-P. E.; von Gunten, U. Oxidation of antibacterial compounds by ozone and hydroxyl radical: Elimination of biological activity during aqueous ozonation processes. *Environ. Sci. Technol.* **2009**, *43* (7), 2498−2504.
(83) Dodd, M. C. Potential impacts of disinfection processes on elimination and deactivation of antibiotic resistance genes during water and wastewater treatment. *J. Environ. Monit.* **2012**, *14* (7), 1754−1771.
(84) Dodd, M. C.; Vu, N. D.; Ammann, A.; Le, V. C.; Kissner, R.; Pham, H. V.; Cao, T. H.; Berg, M.; von Gunten, U. Kinetics and mechanistic aspects of As(III) oxidation by aqueous chlorine, chloramines, and ozone: Relevance to drinking water treatment. *Environ. Sci. Technol.* **2006**, *40* (10), 3285−3292.
(85) Dodd, M. C.; Buffle, M.-O.; von Gunten, U. Oxidation of antibacterial molecules by aqueous ozone: moiety-specific reaction kinetics and application to ozone-based wastewater treatment. *Environ. Sci. Technol.* **2006**, *40* (6), 1969−1977.
(86) Dai, N.; Mitch, W. A. Controlling nitrosamines, nitramines, and amines in amine-based CO_2 capture systems with continuous ultraviolet and ozone treatment of washwater. *Environ. Sci. Technol.* **2015**, *49* (14), 8878−8886.
(87) von Gunten, U. Ozonation of drinking water: Part II. Disinfection and by-product formation in presence of bromide, iodide, or chlorine. *Water Res.* **2003**, *37*, 1469−1487.
(88) *Chemistry of aqueous ozone and transformation of pollutants by ozonation and advanced oxidation processes* Hrubec, J. H., Ed.; Springer-Verlag: Berlin, 1998.
(89) Liu, C.; Croué, J. P. Formation of bromate and halogenated disinfection byproducts during chlorination of bromide-containing waters in the presence of dissolved organic matter and CuO. *Environ. Sci. Technol.* **2016**, *50* (1), 135−144.

DOI: 10.1021/acs.est.8b07225
Environ. Sci. Technol. 2019, 53, 4450−4459